Journal of
Water & Climate Change

IWA PUBLISHING

Journal of Water and Climate Change Vol 15 No 2, 686 doi: 10.2166/wcc.2024.541

Selection of representative general circulation models under climatic uncertainty for Western North America

Seyed Kourosh Mahjour[a,*], Giovanni Liguori[b] and Salah A. Faroughi[a]

[a] Geo-Intelligence Laboratory, Ingram School of Engineering, Texas State University, San Marcos, TX 78666, USA
[b] Department of Biological, Geological, and Environmental Sciences, Alma Mater Studiorum - University of Bologna, Bologna, Italy
*Corresponding author. E-mail: mahjour@txstate.edu

ABSTRACT

Climate change research uses an ensemble of general circulation model runs (GCMs-runs) to predict future climate under uncertainties. To reduce computational costs, this study selects representative GCM-runs (RGCM-runs) for Western North America (WNA) based on their performance in replicating historical climate conditions from 1981 to 2005 and projecting future changes from 1981–2010 to 2071–2100. This evaluation is conducted under two representative concentration pathways (RCPs) scenarios, RCP4.5 and RCP8.5, from the Coupled Model Intercomparison Project 5. By using an envelope-based selection technique and a multi-objective distance-based approach, we identify four RGCM-runs per RCP representing diverse climatic conditions, including wet-warm, wet-cold, dry-warm, and dry-cold. Compared to the full-set, these selected runs show a decreased mean absolute error (MAE) between the reference and RGCM-runs concerning the monthly average mean air temperature ($\bar{T}$) and precipitation ($\bar{P}$). For RCP4.5, $\bar{T}$ MAE is 0.45 (vs. 0.58 in the full-set) and $\bar{P}$ MAE is 0.31 (vs. 0.42). For RCP8.5, $\bar{T}$ MAE is 0.51 (vs. 0.75) and $\bar{P}$ MAE is 0.25 (vs. 0.36). The lower MAE values in the RGCM-run set indicate closer alignment between predicted and reference values, making the RGCM-run suitable for climate impact assessments in the region.

Key words: climate change, climatic uncertainty, general circulation models, model-run reduction, representative model-runs, Western North America

HIGHLIGHTS

- Pioneered a multistep framework for representative general circulation model run (RGCM-run) selection in Western North America, considering computing limitations and ensuring diverse climatic scenarios.
- Compared temperature and precipitation variability under RCP4.5 and RCP8.5, aiding decision-making in the context of climate change.
- Demonstrated substantial reduction in mean absolute error for vital climatic variables using selected RGCM-runs, reducing uncertainty.

1. INTRODUCTION

Understanding the potential impacts of climate change on a global and regional scale is essential for formulating comprehensive resilience plans to mitigate its consequences. Climate change has been identified as a global threat, affecting various sectors and regions differently (Abbass *et al.* 2022). The increasing frequency of extreme weather events, such as hurricanes, droughts, and floods, poses significant challenges to people across the world. It is important to analyze the evolving climate impact on specific regions or sectors and develop customized resilience-building strategies to prepare for and recover from disasters (Zwiers *et al.* 2013). In addition, the assessment of the impacts of climate change at different levels of global warming informs national and international policy discussions around mitigation targets (Arnell *et al.* 2019). This underscores the importance of improving resilience to climate and natural disasters at both the national and international levels.

The US Historical Climatology Network (USHCN) database analysis from 1990 to 2020 in Western North America (WNA) reveals significant temperature and precipitation changes (Bonfils *et al.* 2008; Rosen & Guenther 2015). Advanced numerical tools, such as Earth system models (ESMs) and general circulation models (GCMs), play an important role in quantitatively understanding climate change impacts (Chang *et al.* 2018; Doulabian *et al.* 2021). With 61 distinct GCMs in the Coupled Model Intercomparison Project 5 archive, the ensemble of GCMs evolves to represent potential future climate, incorporating finer resolutions and more processes (Taylor *et al.* 2012; Gulizia & Camilloni 2015). Ensemble GCMs provide a more reliable

representation of potential climate changes, capturing uncertainties related to natural variability, socioeconomic developments, and model discrepancies (Kaini *et al.* 2020; Parding *et al.* 2020). However, the growing number of GCMs poses computational challenges for climate impact research (Gopal Shrestha & Pradhanang 2022). Various model reduction techniques are emerging to address these challenges, preserving essential GCM ensemble characteristics while enhancing efficiency and usability (Senatore *et al.* 2022; Thi Huong *et al.* 2023). These reductions utilize two primary methodologies: the past-performance approach and the envelope-based approach (Seager *et al.* 2007; Pierce *et al.* 2009; Biemans *et al.* 2013).

The past-performance approach involves selecting GCM-runs based on their ability to accurately simulate past and present climate conditions. This approach assumes that models that have performed well in the past are more likely to provide reliable projections of future climate change (Biemans *et al.* 2013; Parding *et al.* 2020). However, the past-performance approach may result in a limited range of future projections. This is because models that are not as skilled at simulating both present and past climate conditions may be excluded from the reduction process, potentially resulting in the absence of plausible future scenarios (Pierce *et al.* 2009). The enveloped-based approach involves selecting models that cover a broad range of projections for one or more climatological variables of interest. This approach seeks to account for the potential futures as predicted by the entire collection of GCMs (Immerzeel *et al.* 2013). Nevertheless, one disadvantage of using this approach is that it does not take into account the skill of the models to accurately predict both the present and the past climates (Lutz *et al.* 2016b). As a result, some models that are less reliable in simulating both present and past climate conditions may be included in the selection, potentially leading to less accurate projections of future climate changes. Lutz *et al.* (2016b) developed an approach that integrates the past-performance and envelope approaches to select representative general circulation model runs (RGCM-runs), reproducing both the simulations of past climatic conditions and the projected changes in key climate variables. This methodology, referenced in various studies (Kaini *et al.* 2020; Gopal Shrestha & Pradhanang 2022), involves selecting RGCM-runs covering diverse climate variables. By evaluating their performance in capturing climatic changes, including extreme indices and historical datasets, these chosen RGCM-runs are deemed suitable for conducting climate impact assessments and crafting adaptation plans. This integrated approach is crucial in climate research, especially for evaluating the effects of climate change on various infrastructures and environments.

In this study, we aim to select RGCM-runs based on their ability to simulate past and future climate changes under two representative concentration pathway (RCPs) scenarios, RCP4.5 and RCP8.5. Our approach follows Lutz *et al.* (2016b), but using a distinct multi-objective distance-based history matching technique. Also, this study distinguishes itself by applying the envelope-based method for the selection of RGCM-runs in the WNA region. We evaluate an initial set of 105 and 77 GCM-runs for RCP4.5 and RCP8.5, respectively, using three criteria: (i) capturing changes in the monthly mean precipitation and air temperature; (ii) capturing changes in the monthly mean extreme indices; and (iii) matching the historical and reference datasets (i.e., history matching). This framework selects a sub-set of four RGCM-runs for each RCP to represent the full set and capture different types of climatic conditions, including wet-warm, wet-cold, dry-warm, and dry-cold scenarios, which represent the extremes of the climatic spectrum. The selection of RGCM-runs for WNA is imperative to enhance our understanding of how climate change will impact this region specifically. The rest of this article is organized as follows: Section 2 provides a background for the study area and discusses the data sources used in this study. Section 3 describes a five-step workflow including different criteria and scoring to select the RGCM-runs. In Section 4, results from the study area are presented as a form of selected RGCM-runs. Finally, in Section 6, the main conclusions are presented.

2. FOCUS AREA AND DATASETS

2.1. Focus area

In this study, we focus on the WNA region, shown in Figure 1, including the northwestern and western states of the United States, along with the southwestern and western provinces and territories of Canada. Since the 1940s, the average annual temperature in the WNA has risen 1 – –2°C, particularly during the winter and spring seasons (Vincent & Gullett 1999). Temperature reconstructions based on tree-ring data (Opała-Owczarek & Niedźwiedź 2019) indicate that spring temperatures in WNA during the previous 50 years have been greater than any comparable time during the last 900 years (Wang *et al.* 2012). In terms of precipitation patterns, observational evidence underscores significant changes in precipitation patterns within the studied area. For example, in southern Canada, annual precipitation has exhibited an increase ranging from 5 to 35% throughout the period spanning from 1900 to 1998 (Kuttippurath *et al.* 2021). In addition, observational

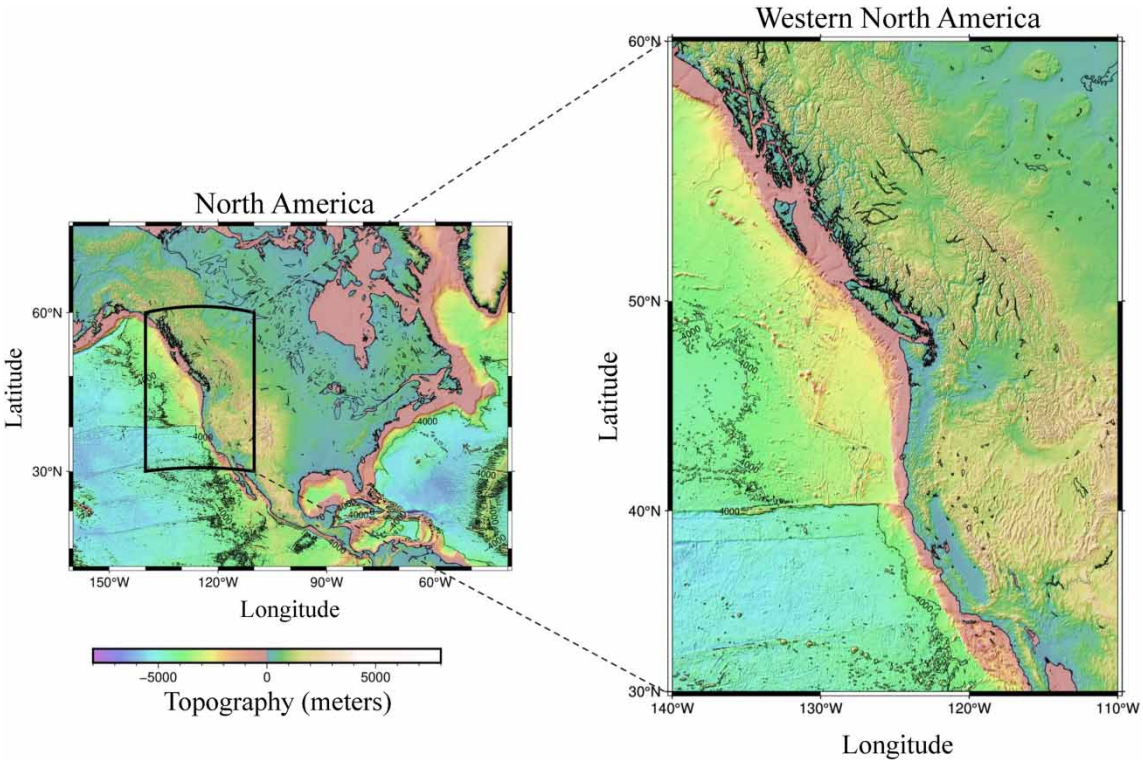

Figure 1 | The topography map of North America. The zoom section shows the study area of WNA covering the northwest and western states of the United States and the southwest and western provinces and territories of Canada.

records indicate a roughly 4% rise in the average annual precipitation across the United States during the period from 1901 to 2015 (Easterling *et al.* 2017).

2.2. Model simulations and reference datasets

Three types of data from WNA are used in this study: (i) *CMIP5 output fields*: The changes in mean air temperature (ΔT) and precipitation (ΔP) simulated by the GCMs of CMIP5 between the two 30-year periods of 1981–2010 and 2071–2100 are obtained. The output resolution of the GCM is $2.5^\circ \times 2.5^\circ$, which has been re-gridded using the Royal Netherlands Meteorological Institute (KNMI) Climate Explorer (Climexp 2023). It is worth noting that the resolution adjustment was made to ensure consistency, given that not all CMIP5 GCMs have a 2.5-degree resolution; (ii) *CMIP5-derived extreme indices*: The extreme indices used for assessing the chosen RGCM-runs are derived from the archive generated by the Expert Team on Climate Change Detection and Indices (ETCCDI) (I CORE and CORE II 2023); and (iii) *Reference datasets*: We employ reference temperature data from the European Centre for Medium-Range Weather Forecasts' global reanalyses, ERA5 (Hersbach *et al.* 2020), and reference precipitation data from the Global Precipitation Climatology Project (GPCP), version 2.3 (Adler *et al.* 2018), to evaluate the selected representative GCMs.

3. METHODOLOGY

The methodology used in this study involves selecting RGCM-runs that cover a wide range of climate scenarios, including both historical and projected future conditions. The workflow, as shown in Figure 2, comprises two main sections: (a) GCM-runs preparation, where we select RCPs that can be used for long-term and short-term climate modeling experiments. We prepare all available GCMs and various runs of a model for each RCP to consider uncertainty in future climate change. During the GCM-run reduction process, it is important to note that GCMs and their multiple runs are often treated as independent options, when in fact they are not entirely independent. This means that runs of a single GCM can be influenced by the same underlying model structures, algorithms, and assumptions; and (b) GCM-runs reduction, where we select the RGCM-runs by evaluating their performance on three criteria: (i) capturing changes in the monthly mean precipitation

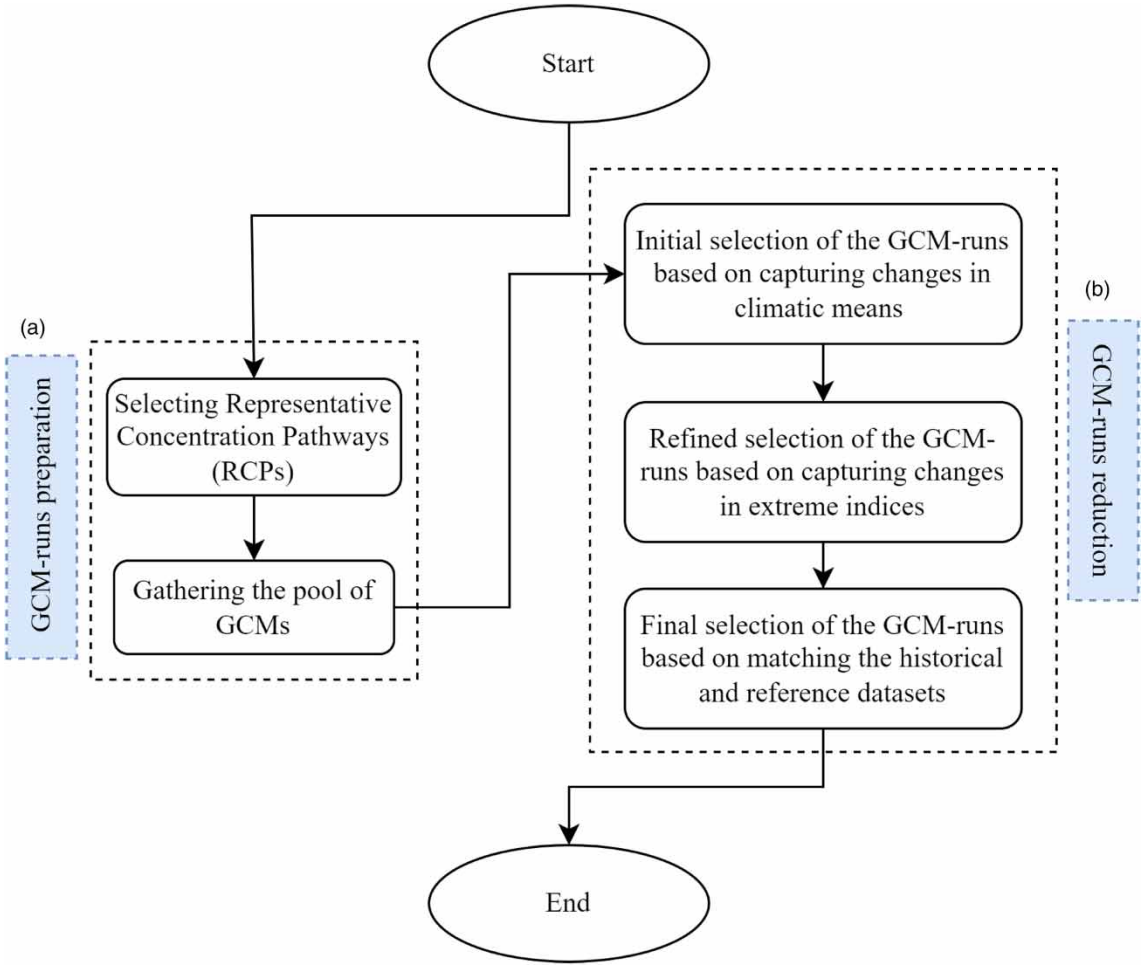

Figure 2 | RGCM-run reduction workflow. The workflow includes two main sections: (a) GCM-runs preparation where we select RCPs, and (b) GCM-runs reduction where we select the RGCM-runs by evaluating their performance on three criteria: (i) capturing changes in the climatology of precipitation and temperature, (ii) capturing changes in the extreme indices, and (iii) matching the historical and reference datasets (i.e., history matching).

and air temperature, (ii) capturing changes in the monthly mean extreme indices, and (iii) matching the historical and reference datasets (i.e., history matching).

3.1. GCM-runs preparation

Four RCPs are utilized for both short-term and long-term experiments in the context of CMIP5 (Peters *et al.* 2013). While each of the four RCPs represents the anticipated radiative forcing levels by 2100 based on the existing literature, practical constraints often lead to trade-offs in climate change impact studies. In this study, we prioritize emission scenarios that cover a wider range of radiative forcing and future temperature anomalies (Van Vuuren *et al.* 2011; Kaini *et al.* 2020). Therefore, we exclude RCP4.5 and RCP8.5 for the GCM-runs collection process. Although our analysis focuses on these two RCPs, the methodology can be adapted to incorporate other pathways. We then use the GCM-runs sourced from CMIP5, emphasizing those that provide area-averaged monthly mean air temperature and monthly total precipitation data. This approach resulted in an initial pool of 77 runs for the RCP8.5 scenario and 105 runs for the RCP4.5 scenario. The GCM-runs listed in Appendix A constitute the foundational dataset for subsequent analyses and play an essential role in selecting RGCM-runs in the WNA region.

3.2. Initial reduction of the GCM-runs

The initial reduction in GCM-runs is established based on projections, indicating changes in mean air temperature (ΔT) and precipitation (ΔP). While it is important to note that different GCM-runs may have varying abilities to project different climate

variables, the approach of considering both ΔT and ΔP together serves several important purposes. First, by evaluating both temperature and precipitation changes, the selection process aims to identify GCM-runs that can effectively represent diverse climate scenarios, including wet-warm, wet-cold, dry-warm, and dry-cold conditions. In addition, the inclusion of both ΔT and ΔP in the selection process helps to ensure that the chosen GCM-runs can capture the interconnected nature of temperature and precipitation changes, which are fundamental components of climate dynamics. This approach acknowledges the complex interactions between temperature and precipitation in shaping climate patterns and allows for the identification of GCM-runs that demonstrate a balanced representation of these important variables. Furthermore, the consideration of both ΔT and ΔP aligns with the goal of selecting RGCM-runs that can provide reliable projections of future climate changes across a range of climatic variables. By incorporating both temperature and precipitation in the selection criteria, the methodology aims to identify GCM-runs that are capable of capturing the multi-faceted nature of climate change, thereby enhancing the robustness and comprehensiveness of the selected ensemble.

The climatic changes are averaged over the $2.5^\circ \times 2.5^\circ$ grid cells within the WNA region between the periods of 1981–2010 and 2071–2100. To begin the selection of the initial sub-set of GCM-runs, we compute the ΔT (in degrees Celsius) and ΔP (as a percentage) between the aforementioned time intervals. ΔT is calculated as the difference between the mean temperature of the two time periods, and ΔP is calculated as the difference between the mean precipitation of the two time periods, expressed as a percentage change. For each GCM, we calculate the mean ΔT and ΔP by averaging the changes across the members of the ensemble, assigning equal weight to each model. We then determine the 10th and 90th percentile values of ΔT and ΔP for RCP4.5 and RCP8.5 GCM-runs (Wondmageghu Tenfie *et al.* 2022). These values represent the four corners of a two-dimensional projection of temperature versus precipitation changes. The choice of the 10th and 90th percentile values is intended to capture the range of variability in the projected changes in temperature and precipitation while disregarding outliers. The 10th percentile values for ΔT and ΔP indicate the 'cold and dry' part of the spectrum. The 10th percentile value for ΔT and the 90th percentile value for ΔP represent the 'cold and wet' part of the spectrum. The 90th percentile value for ΔT and the 10th percentile value for ΔP represent the 'warm and dry' part of the spectrum. The 90th percentile values for ΔT and ΔP indicate the 'warm and wet' part of the spectrum. We use the Euclidean distance metric (You *et al.* 2022) to determine the proximity of each GCM-run's percentile rank scores to the corners of the projection space for ΔT and ΔP within the full ensemble. The Euclidean distance is defined as follows:

$$d = \sqrt{(x_2 - x_1)^2 + (y_2 - y_1)^2} \tag{1}$$

where d is the Euclidean distance between two points (x_1, y_1) and (x_2, y_2) (Mahjour *et al.* 2021a, 2021b). Figure 3 provides a visual representation of the distribution of GCM-runs concerning ΔT and ΔP. Each data point in the figure corresponds to an individual GCM-run and reflects its positioning in a two-dimensional space defined by the ΔT (y-axis) and ΔP (x-axis). The placement of these data points demonstrates their proximity to the corners of the projection space, representing specific percentile rank scores for ΔT and ΔP within the full GCM ensemble. The Euclidean distance metric is used to determine the proximity of each GCM-run's percentile rank scores to the corners of this projection space.

From the ensemble, we select the five GCM-runs for each corner that possess the lowest Euclidean distance and monthly data. Lutz *et al.* (2016b) used five models because they found that this number provided a sufficient range of probable outcomes while still keeping the computational requirements manageable. Following their approach, we also use five models in our study. It is worth mentioning that the reduction of models is restricted to those with daily data, as this is necessary for future decision-making processes and statistical downscaling of GCM-runs at a later stage (Lutz *et al.* 2016b). In this study, the availability of daily data for the temperature and precipitation is examined at the Climate4impact portal (Climate4impact 2023). The initial reduction process results in the selection of 20 GCM-runs for each RCP (i.e., five model-runs for each of the four corners).

3.3. Refined reduction of the GCM-runs

The refined GCM-run reduction procedure is based on the predicted monthly mean changes in the indices of extreme climatic conditions. According to the Special Report on Extreme Events (SREX) of the Intergovernmental Panel on Climate Change (Seneviratne *et al.* 2021), extreme climatic events and changes are particularly significant due to their potentially catastrophic impact on humanity and ecosystems. To perform the refined reduction process, we focus on extreme temperature and precipitation events. To do this, we use the ETCCDI for air temperature and precipitation. For air temperature, the warm spell

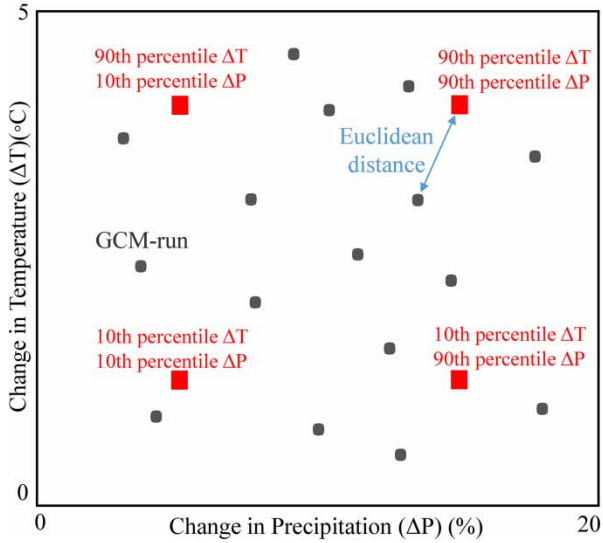

Figure 3 | Schematic distribution of GCM-runs in two-dimensional ΔT-ΔP space. Calculating ΔT and ΔP involves determining differences in the average monthly mean climate variables between the second and first 30-year periods and dividing these differences by the average values of the initial 30-year period (Lutz *et al.* 2016a).

duration index (WSDI) indicates the number of days in at least 6 days when the daily maximum temperature TX_{ij} exceeds the 90th percentile. The cold spell duration index (CSDI) signifies the number of days in at least six days when TX_{ij} falls below the 10th percentile. On the other hand, for precipitation, the consecutive dry day (CDD) represents the maximum duration of dry spells ($P < 1$ mm), and the R99pTOT signifies the precipitation resulting from highly wet days exceeding the 99th percentile (Lutz *et al.* 2016b).

To begin with, we compute these four indices for each year in both the future period (2071–2100) and the past period (1981–2010) within the study area using the database compiled by Sillmann *et al.* (2013). For models not in the database, GCM-runs are downloaded from the climate4impact portal (Climate4impact 2023) and ETCCDI indices are computed using the Max-Planck Institute for Meteorology's Climate Data Operator (CDO-version 1.6.4) (Kaini *et al.* 2020). The indices need to be averaged over a period of 30 years, and the difference in their averages indicates variability in climate extremes. The GCM-runs are then selected based on the climatic indices that are most appropriate for the ensemble corner in which they are situated. In the Warm-Dry projection corner, the selected indices are WSDI and CDD. Moving to the Warm-Wet corner, the chosen indices are WSDI and R99pTOT. On the Cold-Wet corner, the selected indices are CSDI and R99pTOT. Finally, in the cold-dry corner, the chosen indices are CSDI and CDD. For the initial selection of five models for each corner, the two relevant indices are ranked and assigned values ranging from 1 to 5. The final score for each GCM-run is obtained by averaging the two scores given to the indices. Based on this final score, the two highest scores are considered to select the GCM-runs for the next step of GCM reduction.

3.4. Final reduction of the GCM-runs

The final GCM-run reduction procedure evaluates the GCM-runs based on their ability to simulate the monthly mean air temperature and precipitation, which are calculated annually during the reference period spanning from 1981 to 2005 (i.e., history matching). The reference period refers to a specific time frame in the past for which we have observed climate data that can be used to assess the performance of GCM-runs (Mendlik & Gobiet 2016). We compare the GCM-runs to reference datasets and evaluate their capability to reproduce crucial climate characteristics. The reference datasets used for this evaluation include temperature data from ERA5, a global reanalysis dataset from the European Centre for Medium-Range Weather Forecasts, and precipitation data from version 2.3 of the GPCP. These datasets cover the reference period from 1981 to 2005. To determine the skill score, we use a multi-objective distance-based approach that measures the Euclidean distance between the GCM-runs selected from the refined reduction step and reference datasets for temperature and precipitation, taking into account monthly values within the 25-year reference period. We first normalize the air temperature and

precipitation values from both the GCM-runs and the reference datasets to a standardized range of zero to one by Chai & Draxler (2014),

$$X_{\text{normalized}} = \frac{X - X_{\min}}{X_{\max} - X_{\min}} \tag{2}$$

where X is the climate variable to be normalized, $X_{\text{normalized}}$ is the normalized value, $X_{\min}$ is the minimum value of X, and $X_{\max}$ is the maximum value of X. Afterward, we compute the Euclidean distance between the normalized data of the GCM-runs and the reference datasets for temperature (T-distance) and precipitation (P-distance) separately. We then use a multi-objective approach by averaging these distances, thereby incorporating both precipitation and temperature metrics to determine the skill scores of GCM-runs. At each corner, the GCM-run with the lowest average normalized distance is selected, indicating the smallest deviation from the reference value. To evaluate the effectiveness of our distance-based approach in selecting the final RGCM-runs based on the past performance of GCM-runs, the mean absolute error (MAE) is used, which is defined by,

$$\text{MAE} = \frac{1}{n}\sum_{i=1}^{n} |p_i - \bar{p}| \tag{3}$$

where n is the number of samples or observations, p_i is the predicted value of the *ith* sample or observation, and $\bar{p}$ is the true value of the *ith* sample or observation (Hodson 2022). The purpose of this comparison is to assess the closeness of the behavior of the RGCM-run set to the actual values. To interpret the results of this comparison, we look at the magnitude of the MAE for each set. If the MAE for the RGCM-run set is smaller than the MAE for the full-sets, this would suggest that the behavior of the RGCM-run set is closer to the actual values. By following this procedure, one RGCM-run is selected from each corner, resulting in four RGCM-runs from each RCP. These can be used reliably in climate impact assessments under uncertainty.

4. RESULTS AND DISCUSSION

The initial GCM-run selection process is based on the projected changes in ΔT and ΔP between the periods of 1981–2010 and 2071–2100. For each GCM-run, we calculate its distance to the 10th and 90th percentile values in the corners. Subsequently, we choose the five GCM-runs with the shortest Euclidean distance to each corner. Figure 4 represents the outcome of this initial GCM-run reduction for each RCP, with a primary focus on capturing mean climate changes. Gray circles represent the model-runs not chosen for the subsequent GCM reduction stage. The chosen GCM-runs' proximity to the 10th and 90th percentiles (red symbols) may vary significantly. For example, the GCM-runs selected for the warm and dry corner of RCP8.5 are relatively close to the corner, while several models chosen for the cold and wet corner are at a considerable distance. This difference is partly due to the limited availability of GCM-runs with daily output. In Figure 4, gray circles represent GCM-runs that are not selected for the subsequent stage of GCM reduction. These models cannot meet the criteria set for proximity to the 10th and 90th percentile values. From the initial 105 GCM-runs of RCP4.5 and 77 GCM-runs of RCP8.5, a total of 20 model-runs were selected for each RCP. Furthermore, in the RCP4.5 initial GCM pool, the ΔT ranges from 0.8 to 3.8°C, and ΔP ranges from –2.8 to 13.2%. For the RCP8.5 initial GCM pool, ΔT ranges from 2.78 to 6.31°C, and ΔP ranges from –0.39 to 23.50%. The variability in the projections of ΔT and ΔP is markedly higher for the RCP8.5 model pool due to substantially higher greenhouse gas emissions in the RCP8.5 scenario, resulting in increased radiative forcing and more pronounced changes in temperature and precipitation.

In the next step of the GCM-run reduction process, the changes in the four defined ETCCDI indices between 1981–2010 and 2071–2100 are calculated for the GCM-runs that remained after the initial GCM-run reduction (total of 20 for each RCP). The results obtained from the refined selection step are shown in Figure 5(a)–(d) for RCP4.5 and Figure 5(e)–(h) for RCP8.5, considering the relevant indices. The refined reduction of GCM-runs was based on the two highest averaged rank scores. In cases where two or three GCM-runs possess identical highest or second-highest averaged rank scores, they are also chosen. Accordingly, 10 GCM-runs out of 20 were selected for each RCP. In RCP4.5, the following selections were made: for warm–dry, CSIRO-Mk3-6-0.r10i1p1 and BNU-ESM.r1i1p1 were chosen; for warm–wet, CanESM2.r1i1p1, CanESM2.r3i1p1, and CSIRO-Mk3-6-0.r1i1p1 were selected; for cold–wet, CCSM4.r4i1p1 and GISS-E2-R.r6i1p1 were chosen; and for cold–dry,

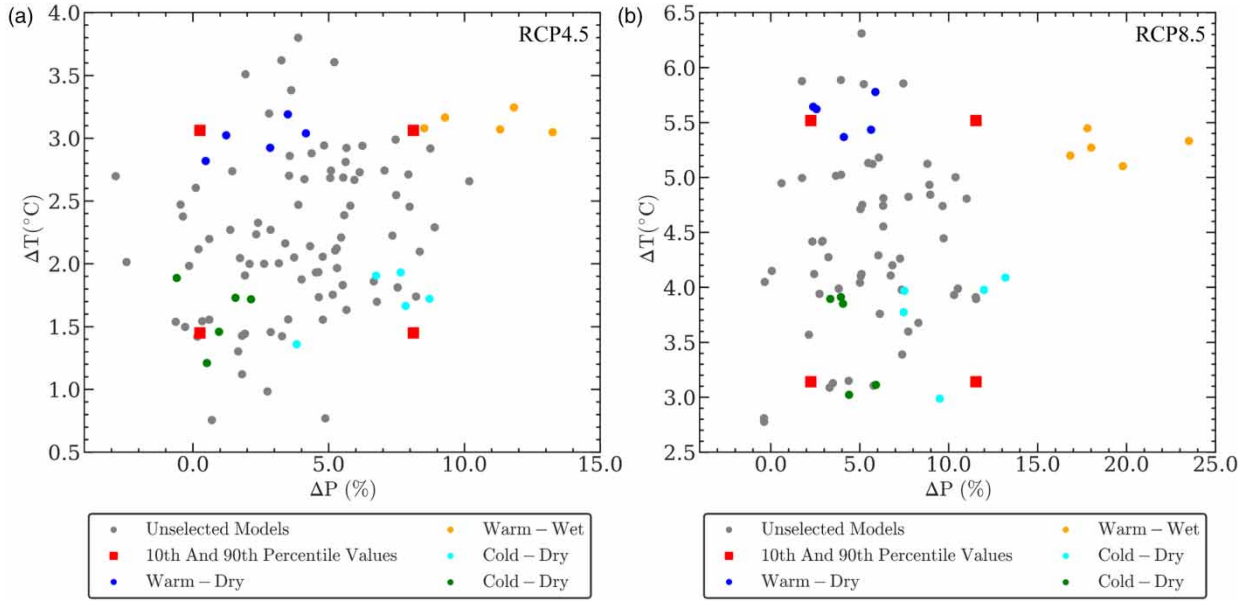

Figure 4 | Scatter plots of changes in mean air temperature (ΔT) versus changes in precipitation (ΔP) projected for the GCM-runs in (a) RCP4.5 and (b) RCP8.5 between 2071 and 2100, and 1981 and 2010. The variation in projected ΔT and ΔP is significantly greater for the RCP8.5 model pool compared to the RCP4.5 model pool. The 10th and 90th percentile values (corners of the full climatic spectrum) for ΔT and ΔP are highlighted by red symbols. Gray circles reflect the model-runs that were not chosen for the next stage of GCM reduction. The GCM-runs are selected that demonstrate minimum distance from the 10th and 90th percentile values of ΔT (°C) and ΔP (%), while possessing daily data. From the 105 GCM-runs of RCP4.5 and 77 GCM-runs of RCP8.5, we selected a total of 20 model-runs for each RCP.

CCSM4.r3i1p1, GFDL-ESM2M.r1i1p1, and MPI-ESM-MR.r3i1p1 were selected. On the other hand, in RCP8.5, the selections were as follows: for warm–dry, HadGEM2-AO.r1i1p1, HadGEM2-ES.r4i1p1, and IPSL-CM5A-LR.r1i1p1 were chosen; for warm–wet, CanESM2.r1i1p1 and CanESM2.r2i1p1 were selected; for cold–wet, CNRM-CM5.r1i1p1 and MRI-CGCM3.r1i1p1 were chosen; and for cold–dry, CCSM4.r2i1p1, GFDL-ESM2M.r1i1p1, and inmcm4.r1i1p1 were selected. It is important to note that this approach to calculating an averaged rank score may exclude GCM-runs with the greatest change in one ETCCDI index due to the lowest change in another. For example, in the warm and dry corner, the model HadGEM2-ES.r4i1p1 in RCP4.5 predicts the most substantial increases in CDD. Nevertheless, it was not selected due to a lower averaged rank score compared to CSIRO-Mk3-6-0.r10i1p1 and BNU-ESM.r1i1p1, which had higher averaged rank score, even though they did not project the same level of increase in CDD. Figure 6 illustrates that GCM-runs that exhibit significant changes in mean air temperature also display notable changes in extreme weather events. This trend is evident across the 20 GCM-runs from the initial selection of each RCP, as well as the full-set of GCM-runs. The extent of change in the indices, as indicated by the shadow colors in the figure, is closely associated with changes in temperature and precipitation in both GCM-run sets. This is because extreme events are often caused by the same underlying factors that produce fluctuations in means, such as atmospheric circulation, ocean currents, and land use. For example, higher temperatures can increase the frequency and intensity of heat waves and the likelihood of droughts in some areas, as well as heavy rainfall in others. In both RCP scenarios from the 20 GCM-runs and the full-set, models that project the greatest increases in mean air temperature also show the largest increases in warm spells and the most significant declines in cold spells, see Figure 6(a), (b), (e), and (f). For precipitation, the general correlation between models that exhibit a larger increase in total precipitation and those that predict a greater increase in precipitation on extremely wet days holds for both RCPs, see Figure 6(c), (d), (g), and (h)). In addition, the selected GCM-runs in this stage indicate that the CSDI is projected to decrease by 50.2–86.4% based on RCP4.5 and by 87.8–98.3% based on RCP8.5. This shows that future nights are expected to be warmer (Paul & Maity 2023). The WSDI is projected to increase by 603.9–1331.4% for RCP4.5 and 894.1–1,475.5% for RCP8.5. An increase in WSDI indicates a rise in future maximum temperatures compared to the past. The majority of ensemble members predict that the CDD and R99pTOT will increase for both RCPs, showing that there will be more heatwaves, storms, and floods in the WNA in the coming decades. Detailed information regarding the changes in index values is provided in Appendix B.

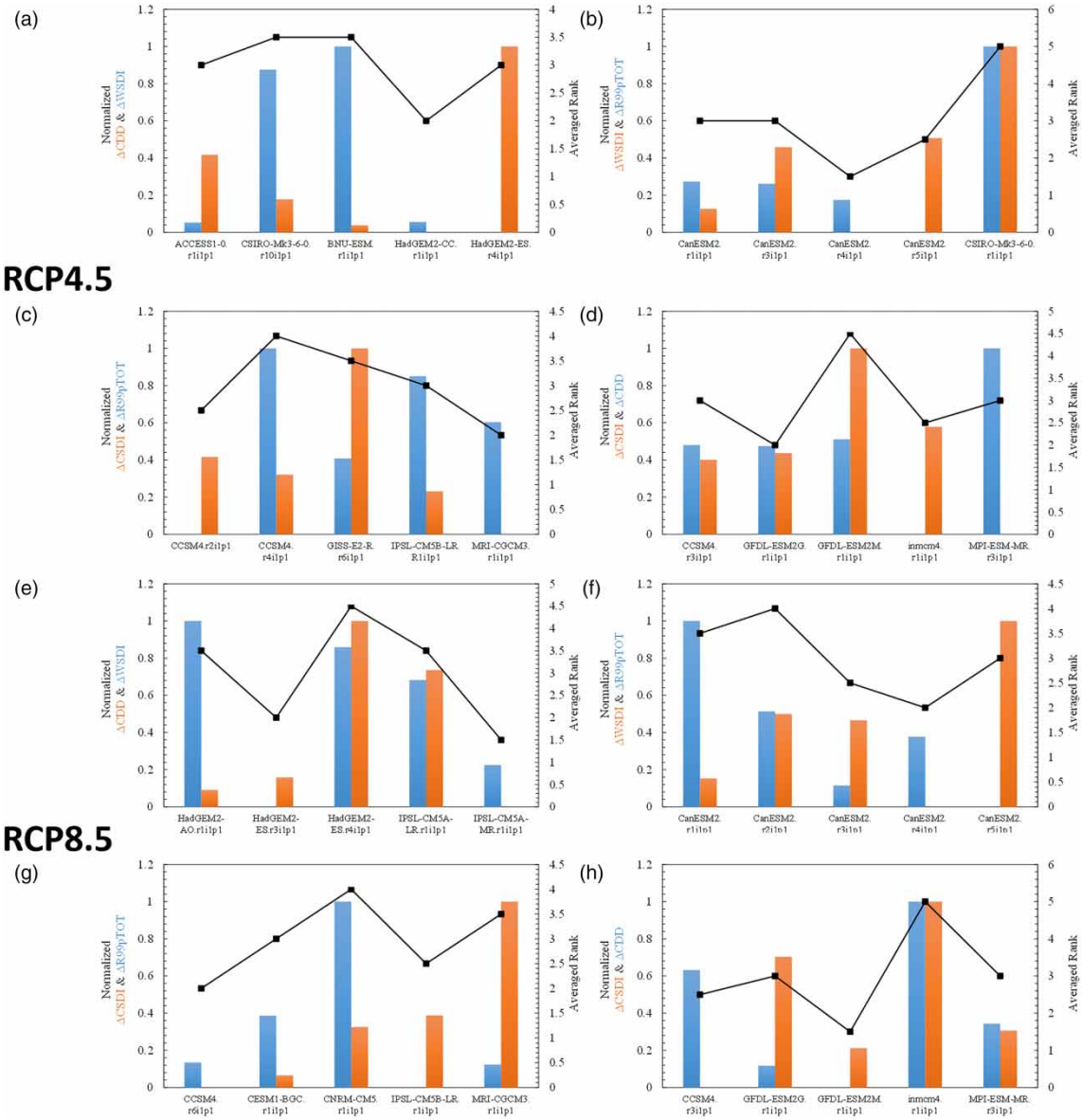

Figure 5 | Refined selection of the GCM-runs from the ensembles of RCP4.5 (a)–(d), and RCP8.5 (e)–(h) based on the relevant indices. To obtain the final score for each GCM-run, the two relevant indices are scored and averaged (shown in black color). The two highest final scores are then used to choose two or three GCM-runs from a total of five GCM-runs in each corner. Calculating the average rank helps to eliminate models that exhibit the greatest change in one ETCCDI index but the lowest change in another. During the refined selection, 10 GCM-runs were selected out of 20.

Figure 7 depicts the seasonal mean changes in temperature and precipitation for three sets of GCM-runs: (i) the initial ensemble GCM-runs, comprising 77 model-runs for RCP8.5 and 105 model-runs for RCP4.5; (ii) 20 GCM-runs for each RCP obtained from the initial selection process based on the changes in climatic means; and (iii) 10 GCM-runs for each RCP obtained from the refined selection process based on the changes in extreme indices. The results show that, across the GCM-runs and months, there is a consistent trend of mean changes in temperature and precipitation change for both RCP4.5 and RCP8.5 scenarios. According to Figure 7(a) and (c), the mean air temperature changes depicted across the GCM-run sets are observed to be consistent for the months under both RCP4.5 and RCP8.5 scenarios. This suggests a similarity in the projected temperature changes regardless of the size of the GCM-run sub-set selected. In Figure 7(b) and (d), the analysis of precipitation changes between August and December reveals similar average changes for both RCPs across the

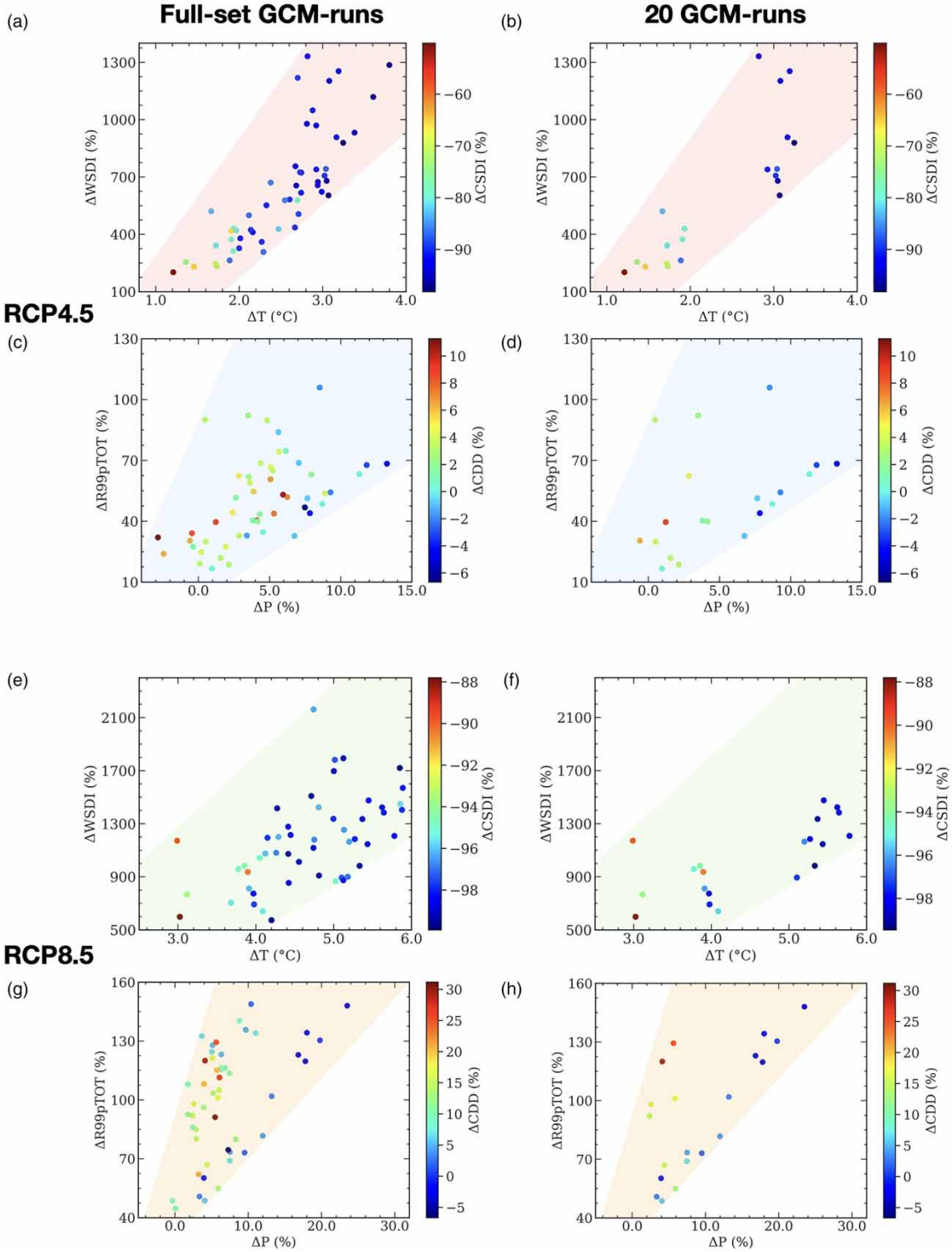

Figure 6 | Changes in projected ΔT, ΔWSDI, and ΔCSDI between 2071–2100 and 1981–2010 for RCP4.5 and RCP8.5 across the full-set of GCM-runs ((a), (c), (e), and (g)) and the 20 GCM-runs from the initial selection ((b), (d), (f), and (h)). The extent of change in the indices, as indicated by the shadow colors in the figure, is closely associated with changes in temperature and precipitation in both GCM-run sets. In both RCPs from the 20 GCM-runs and the full-set, models that project the greatest increases in mean air temperature show the largest increases in warm spells and the most significant declines in cold spells, see (a), (b), (e), and (f). For precipitation, the general correlation between models that exhibit a larger increase in total precipitation and those that predict a greater increase in precipitation on extremely wet days holds for both RCPs, see (c), (d), (g), and (h).

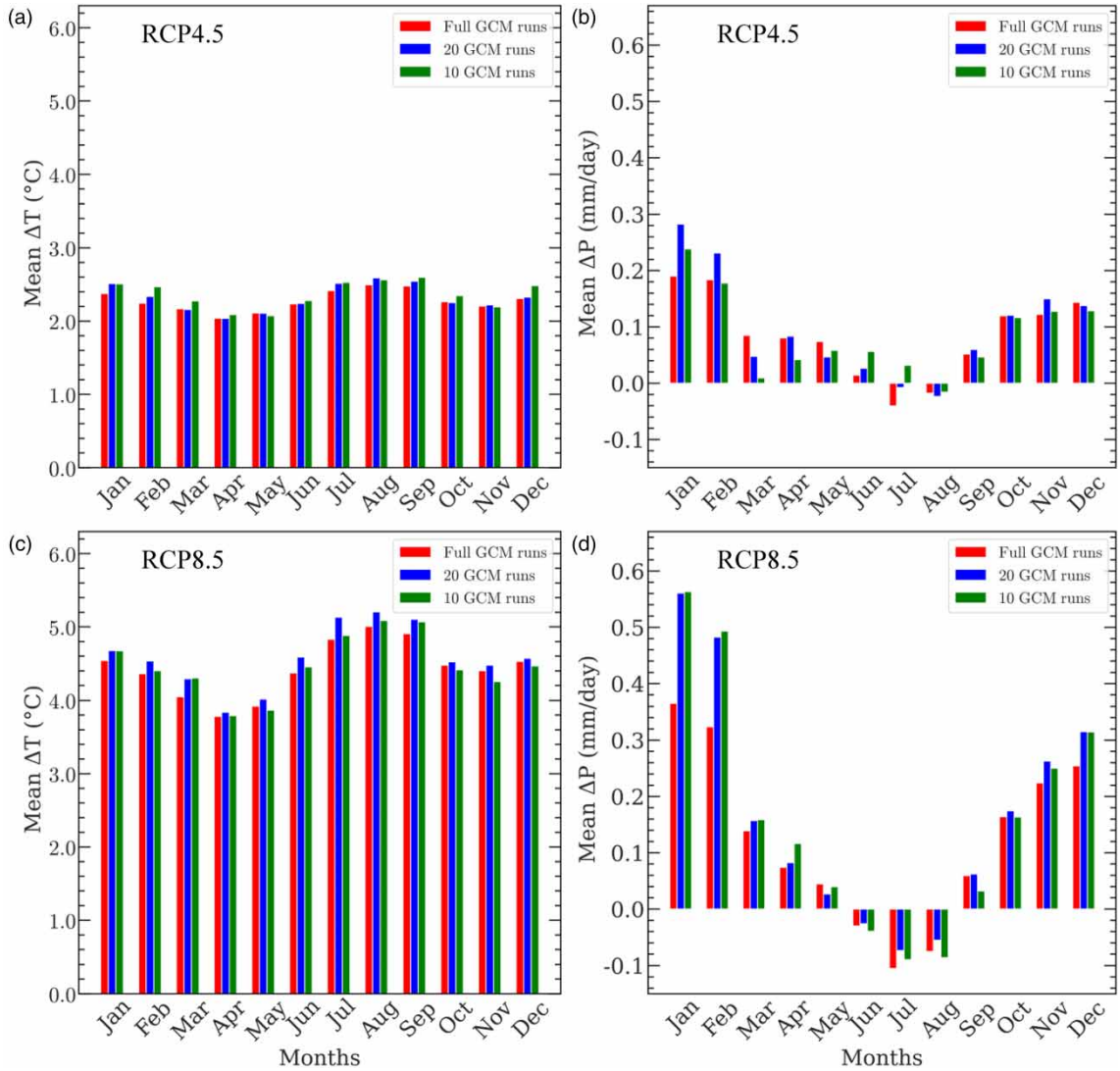

Figure 7 | The seasonal mean changes in temperature and precipitation between 1981–2010 and 2071–2100 for three sets of GCMruns: (i) full ensemble GCM-runs, including 77 and 105 GCM-runs for RCP8.5 and RCP4.5, respectively; (ii) 20 GCM-runs for each RCP obtained from the initial selection process based on the changes in climatic means; and (iii) 10 GCM-runs for each RCP obtained from the refined selection process based on the changes in extreme indices. The mean air temperature change for the sets of GCM-runs is about the same for the months for RCP4.5 and RCP8.5 ((a) and (c)). The analysis of the results shows that the average change in precipitation during the period from August to December is approximately the same for both RCPs ((b) and (d)).

different GCM-run sub-sets. This indicates a certain consistency in projected precipitation alterations irrespective of the ensemble size chosen.

Furthermore, to assess the similarity between the mean change values of the three sets of GCM-runs for all 12 months, we employ a correlation analysis (Menebo 2020). To this end, we arranged the data such that each dataset (mean changes in temperature/precipitation) represents a column, and each row represents a month. The correlation matrix was then calculated to determine the pairwise Pearson's correlation coefficients (Ly *et al.* 2018) between the datasets. A correlation coefficient of 1 indicates a perfect positive correlation (i.e., the two variables move in the same direction), while a coefficient of –1 indicates a perfect negative correlation (i.e., the two variables move in opposite directions). A coefficient of 0 indicates that there is no correlation between the two variables. Four correlation matrices compare the full set of GCM-runs as well as sub-sets of 20 and 10 GCM-runs for mean changes in temperature and precipitation values under each RCP. The analysis for RCP4.5 reveals significantly high similarity in mean values across the GCM-run sets, as evidenced by correlation coefficients

close to 1 for all values. This suggests that even the smaller sub-sets effectively represent the full uncertainty domain. Specifically, for mean temperature changes, the correlation coefficients between the full-set and 20 GCM-runs and between the full-set and 10 GCM-runs are approximately 0.98 and 0.93, respectively. Similarly, for mean precipitation changes, the correlation coefficients are around 0.94 and 0.86 between the full-set and 20 GCM-runs and the full-set and 10 GCM-runs, respectively. Moreover, correlations within the sub-sets of GCM-runs (20 GCM-runs and 10 GCM-runs) are notably high, reaffirming their representativeness. For RCP8.5, the correlation matrix for mean temperature changes in RCP8.5 demonstrates a strong correlation between the complete set and both the 20 and 10 GCM-run sub-sets, with coefficients of 0.98 and 0.96, respectively.

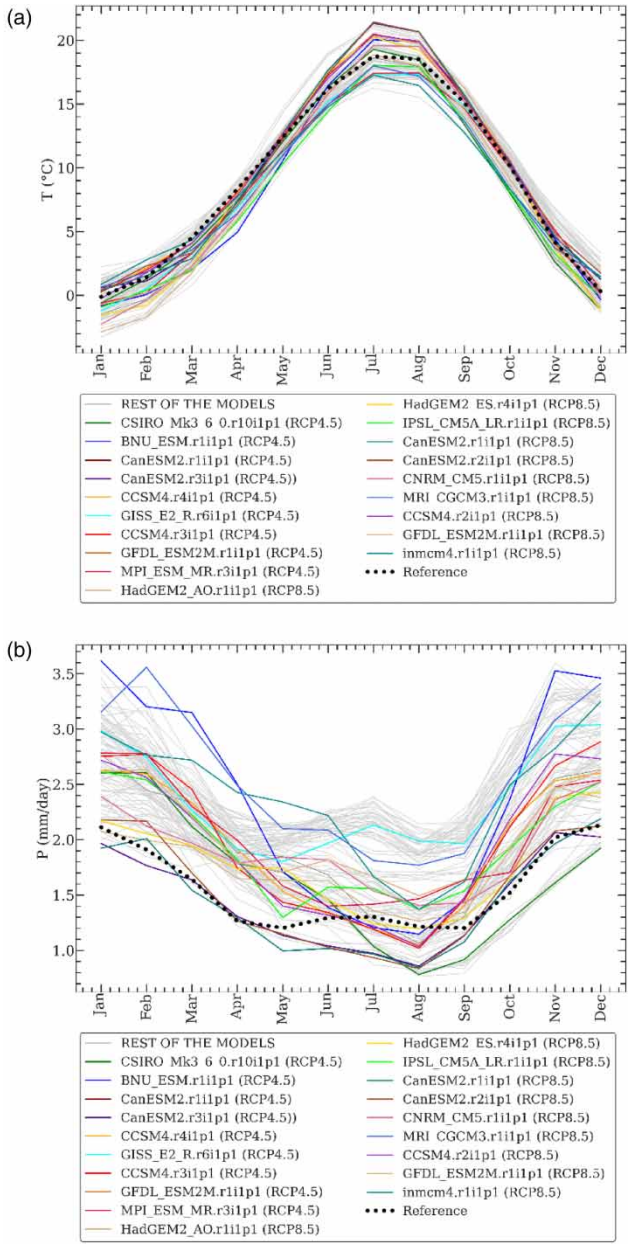

Figure 8 | Monthly averages of (a) mean air temperature ($\bar{T}$) and (b) precipitation ($\bar{P}$) for the reference and the sets of GCM-runs. The reference data sets used for this evaluation include temperature data from ERA5 and precipitation data from GPCP-version 2.3. The GCM-runs obtained from the refined selection step properly captured the full behavior and uncertainty domain of the full-set ensembles. There is also relatively considerable divergence among the models in terms of precipitation compared to temperature, showing a broader range of uncertainty in precipitation and the difficulty of accurate model projection for precipitation.

Similarly, the correlation matrix for mean precipitation changes under RCP8.5 shows strong correlations, reaffirming the effective representation of the full uncertainty domain by the sub-sets, with correlation coefficients of 0.98 and 0.98 for the 20 GCM-runs, and 0.99 and 1 for the 10 GCM-runs, with the complete set. This finding suggests that the GCM-run sub-sets successfully captured the full uncertainty domain.

After checking the selected GCM-runs' projected changes in climatic means and extreme indices, their ability to reproduce the reference precipitation and temperature data is assessed. To this end, precipitation data from GPCP and temperature data from ERA5 for the reference period of 1981–2005 are used. Figure 8 displays the monthly averages of mean air temperature ($\bar{T}$) and precipitation ($\bar{P}$) for the reference and the GCM-runs selected during the refined selection process (10 for each RCP). It is shown that the selected GCM-runs approximately captured the full behavior and uncertainty domain of the full-set ensembles (i.e., 77 GCM-runs for RCP8.5 and 105 GCM-runs for RCP4.5). Despite the complexity and variability of the climatic conditions, these selected runs encompass a spectrum of scenarios akin to the broader ensemble. We also observed that there is considerable variability in precipitation across the models, in contrast to temperature, indicating a wider range of uncertainty in precipitation. Precipitation is influenced by several factors in the WNA such as atmospheric circulation, moisture transport, and terrain, making it more susceptible to uncertainty compared to temperature. As a result, even if we consider multiple climate model-runs, future projections of precipitation patterns can be highly uncertain (Eden *et al.* 2014).

Table 1 reports the final four representative GCM-runs (RGCM-runs) highlighted in blue for RCP4.5 and green for RCP8.5 ensembles. The selection for each corner is based on the least averaged normalized distance (average of precipitation and temperature distances, see Section 3.4.) This method of selection may result in GCM-runs with the lowest P-distance not being chosen due to a high T-distance (or vice versa). For instance, the CanESM2.r3i1p1 is not selected in the warm and dry corner of RCP4.5, as shown in Table 1, despite having the lowest normalized P-distance of zero. This is because it has a relatively high normalized T-distance of 0.53, which results in an average normalized distance of 0.26. On the other hand, the model CSIRO-Mk3-6-0.r1i1p1 has an average normalized distance of 0.17, with a normalized T-distance of 0.20 and a normalized P-distance of 0.15, respectively. Thus, CSIRO-Mk3-6-0.r1i1p1 is chosen because it has the lowest average normalized distance in the cold and dry corners. Accordingly, we selected the RGCM-runs that best matched the reference data for both temperature and precipitation.

As shown in Figure 9, the monthly climatic behavior of the four RGCM-runs from each RCP, in comparison to other sets of model-runs, is closer to the reference when considering the average $\bar{P}$ and $\bar{T}$. The results indicate that for RCP4.5, the MAE of

Table 1 | GCM-runs reduction based on history matching. Distances between GCM-runs and the reference climate dataset for RCP4.5 and RCP8.5 are given for the reference period of 1981–2005. One RGCM-run is selected for each corner, considering the least averaged normalized distance (average of precipitation and temperature distances). The blue color highlights the selected RGCM-runs for RCP4.5 and the green color highlights the selected RGCM-runs for RCP8.5

RCP	Projection	Model	P-distance	T-distance	Normalized P-distance	Normalized T-distance	Averaged normalized distance
RCP4.5	Warm-Dry	BNU-ESM.r1i1p1	20.66	38.99	0.95	0.89	0.92
		CSIRO-Mk3-6-0.r10i1p1	11.19	31.01	0.21	0.05	0.13
	Warm-Wet	CanESM2.r3i1p1	8.54	35.56	0	0.53	0.26
		CSIRO-Mk3-6-0.r1i1p1	10.45	32.43	0.15	0.20	0.17
		CanESM2.r1i1p1	9.62	36.28	0.08	0.61	0.34
	Cold-Wet	CCSM4.r4i1p1	12.74	34.46	0.33	0.41	0.37
		GISS-E2-R.r6i1p1	16.50	31.78	0.62	0.13	0.38
	Cold-Dry	CCSM4.r3i1p1	14.19	30.53	0.44	0	0.22
		MPI-ESM-MR.r3i1p1	12.84	32.44	0.34	0.20	0.27
		GFDL-ESM2M.r1i1p1	12.47	35.50	0.31	0.52	0.42
RCP8.5	Warm-Dry	HadGEM2-ES.r4i1p1	9.41	35.14	0.07	0.49	0.28
		HadGEM2-AO.r1i1p1	10.02	40.02	0.12	1	0.56
		IPSL-CM5A-LR.r1i1p1	12.46	39.27	0.37	0.92	0.61
	Warm-Wet	CanESM2.r2i1p1	8.81	33.80	0.02	0.34	0.18
		CanESM2.r1i1p1	9.62	36.28	0.08	0.61	0.34
	Cold-Wet	CNRM-CM5.r1i1p1	10.33	35.91	0.14	0.57	0.35
		MRI-CGCM3.r1i1p1	21.33	34.31	1	0.40	0.70
	Cold-Dry	GFDL-ESM2M.r1i1p1	12.47	35.50	0.31	0.52	0.42
		inmcm4.r1i1p1	18.32	36.03	0.77	0.58	0.67
		CCSM4.r2i1p1	12.51	34.58	0.31	0.43	0.37

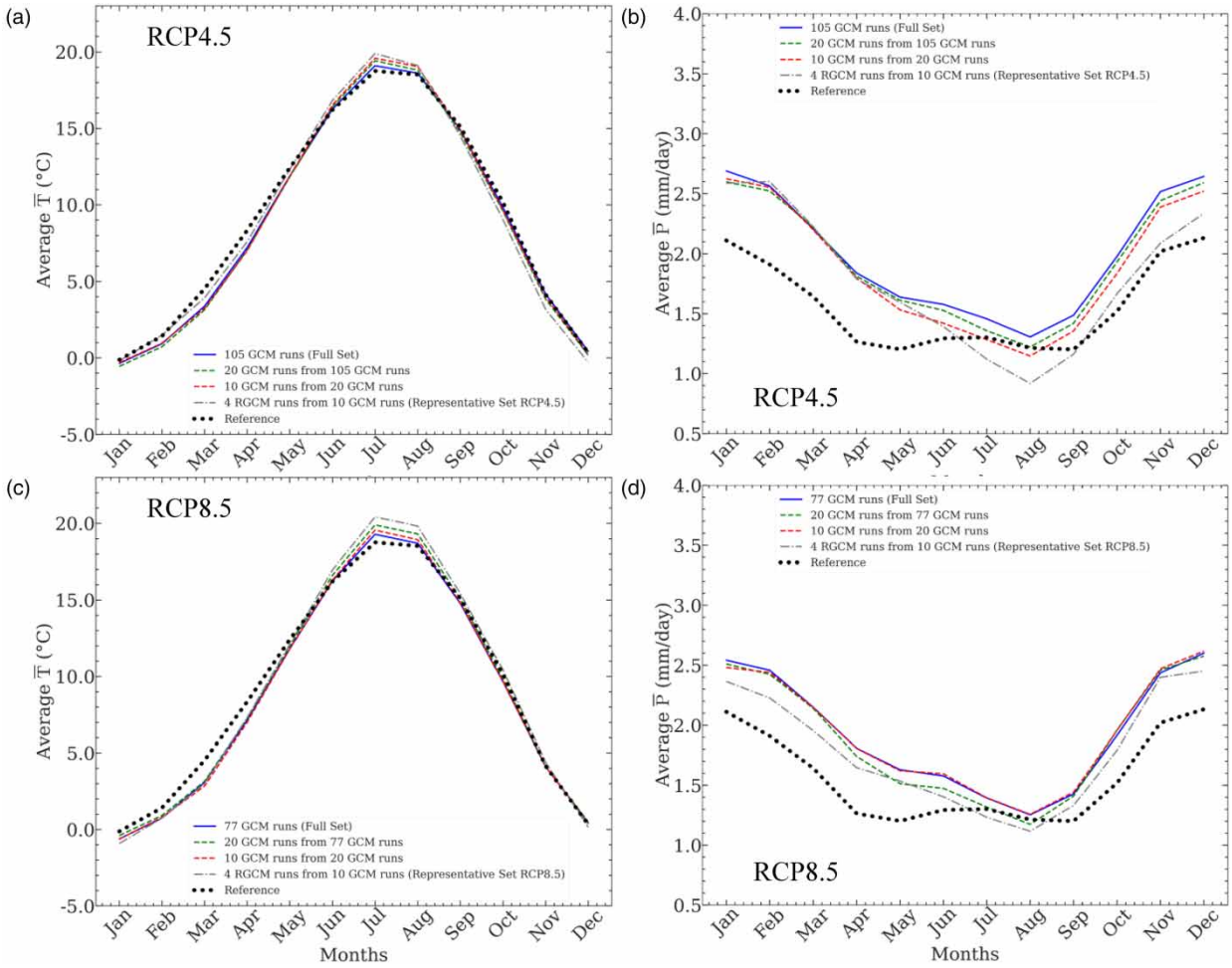

Figure 9 | (a) Average $\bar{T}$ for the model-run sets from RCP4.5. (b) Average $\bar{P}$ for the model-run sets from RCP4.5. (c) Average $\bar{T}$ for the model-run sets from RCP8.5. (d) Average $\bar{P}$ for the model-run sets from RCP4.8. The monthly climatic behavior of four RGCM-runs from each RCP is closer to the reference.

$\bar{T}$ between the reference and RGCM-runs is 0.45, whereas it is 0.58 for the full set. Similarly, for RCP8.5, the MAE of $\bar{T}$ between the reference and RGCM-runs is 0.51, while it is 0.75 for the full set. In $\bar{P}$ for RCP4.5, the MAE between the reference and RGCM-runs is 0.31, while it is 0.42 for the full set. Also, for RCP8.5, the MAE of $\bar{P}$ between the reference and RGCM-runs is 0.25, while it is 0.36 for the full set. Since the MAE for both climatic variables of RCP4.5 and RCP8.5 is lower in the RGCM-run set compared to the full-set, it can be concluded that the model's predictions in the RGCM-runs are closer to the actual values than those in the full set. After thoroughly evaluating a vast pool of GCM-runs in the WNA, we selected the best ones – four RGCM-runs for each RCP. Our approach considers not only the simulations of past climatic conditions but also the projected changes in key climatic and extreme indices in the WNA. Hence, the RGCM-runs for further in-depth study and analysis of climate change in WNA are recommended to pave the way for better adaptation and mitigation measures to climate change.

5. LIMITATIONS AND FUTURE DIRECTIONS

While the current process aims to integrate the most effective aspects of envelope-based and past-performance-based GCM-run reduction for impact assessments, there remain certain sources of error that require attention. The initial error stems from prioritizing the envelope of changes in means, potentially narrowing the ensemble's scope when projecting changes in climatic extremes. As GCM-run reduction based on skill occurs later in the process when fewer GCM-runs are available, the selected ones may not necessarily be the most proficient in simulating past climate. Notably, Figure 8 indicates significant

winter-time biases in temperature and precipitation in the WNA. Hence, downscaling and mitigating biases in selected climate models' future projections become imperative. Another source of error lies in assuming independence among the model-runs, disregarding model interdependence arising from shared code, validation, or forcing data among some models. This is especially relevant in our study, where multiple ensemble members from the same GCM's initial condition ensemble are included. Future research might consider weighing measures based on CMIP5 model interdependence. Moreover, it is crucial to integrate distance-based approaches and envelope-based techniques for different climatic variables in other regions to address uncertainties. The workflow can be improved by comparing CMIP5 and CMIP6 GCM-run results, exploring methods such as fuzzy logic, and integrating downscaling techniques for a more refined selection process. Implementing these enhancements can create a more comprehensive approach, expanding the utility of climate impact studies across different geographical settings.

6. CONCLUSION

This study aimed to select RGCM-runs for WNA under two different RCPs. We evaluated 105 GCM-runs for RCP4.5 and 77 for RCP8.5 from Coupled Model Intercomparison Project 5 (CMIP5). To choose the GCM-runs, we considered the simulated past climate from 1981 to 2005 and projected climatic changes from 1981–2010 to 2071–2100 for each RCP.

In the initial selection step, a subset of 20 GCM-runs for each RCP, with five representing each climatic corner including wet–warm, wet–cold, dry–warm, and dry–cold scenarios, was selected based on the percentiles of temperature and precipitation changes. The variability in temperature and precipitation changes was notably higher for RCP8.5 compared to RCP4.5. For RCP4.5, the temperature ranged from 0.76 to 3.80°C, and precipitation ranged from -2.85% to 13.25%. In contrast, for RCP8.5, the temperature ranged from 2.78 to 6.31°C and precipitation ranged from –0.39 to 23.50%.

In the refined selection step, changes in relevant ETCCDI indices were calculated and ranked for the remaining 20 GCM-runs for each RCP. Ten GCM-runs were chosen based on the highest averaged rank scores for each RCP, indicating notable changes in both mean air temperature and extreme weather events. The selected GCM-runs in this stage showed that the consecutive dry days index (CSDI) was projected to decrease by 50.2–86.4% based on RCP4.5 and by 87.8–98.3% based on RCP8.5. The WSDI was projected to increase by 603.9–1,331.4% for RCP4.5 and 894.1–1,475.5% for RCP8.5. An increase in WSDI indicated a rise in future maximum temperatures compared to the past.

In the final reduction step, a multi-objective distance-based history matching approach was used to select four RGCM-runs for each RCP based on their ability to simulate the monthly average mean air temperature ($\bar{T}$) and precipitation ($\bar{P}$). The RGCM-run set showed a lower MAE for both climatic variables compared to the full set. Specifically, for RCP4.5, the MAE of $\bar{T}$ between the reference and RGCM-runs was 0.45, contrasting with 0.58 for the full set. For RCP8.5, the MAE of $\bar{T}$ was 0.51 compared to 0.75 for the full set. Similarly, for the $\bar{P}$, the MAE between the reference and RGCM-runs was 0.31 for RCP4.5 and 0.25 for RCP8.5, while 0.42 and 0.36 for the full set, respectively. The consistently lower MAE for both climatic variables in the RGCM-run set for RCP4.5 and RCP8.5 indicated that the model's projections in the RGCM-runs are close to the reference values.

After conducting an assessment of a wide range of GCM-runs in the WNA region, the four best-performing RGCM-runs were selected for each RCP, considering past climatic conditions and projected changes in climatic and extreme indices. This subset can aid in developing climate change adaptation and mitigation strategies for the WNA region.

ACKNOWLEDGEMENTS

S. A. F. would like to acknowledge support by the Department of Energy's Biological and Environmental Research (BER) program (award no. DE-SC0023044).

DATA AVAILABILITY STATEMENT

All relevant data are included in the paper or its Supplementary Information.

CONFLICT OF INTEREST

The authors declare there is no conflict.

REFERENCES

Abbass, K., Qasim, M. Z., Song, H., Murshed, M., Mahmood, H. & Younis, I. 2022 A review of the global climate change impacts, adaptation, and sustainable mitigation measures. *Environmental Science and Pollution Research* **29** (28), 42539–42559. https://doi.org/10.1007/s11356-022-19718-6.

Adler, R. F., Sapiano, M. R. P., Huffman, G. J., Wang, J.-J., Gu, G., Bolvin, D., Chiu, L., Schneider, U., Becker, A., Nelkin, E., Xie, P., Ferraro, R. & Shin, D. 2018 The global precipitation climatology project (GPCP) monthly analysis (new version 2.3) and a review of 2017 global precipitation. *Atmosphere* **9** (4), 138. https://doi.org/10.3390/atmos9040138.

Arnell, N. W., Lowe, J. A., Challinor, A. J. & Osborn, T. J. 2019 Global and regional impacts of climate change at different levels of global temperature increase. *Climatic Change* **155**, 377–391. https://doi.org/10.1007/s10584-019-02464-z.

Biemans, H., Speelman, L. H., Ludwig, F., Moors, E. J., Wiltshire, A. J., Kumar, P., Gerten, D. & Kabat, P. 2013 Future water resources for food production in five South Asian river basins and potential for adaptation—A modeling study. *Science of the Total Environment* **468**, S117–S131. https://doi.org/10.1016/j.scitotenv.2013.05.092.

Bonfils, C., Santer, B. D., Pierce, D. W., Hidalgo, H. G., Bala, G., Das, T., Barnett, T. P., Cayan, D. R., Doutriaux, C., Wood, A. W., Mirin, A. & Nozawa, T. 2008 Detection and attribution of temperature changes in the mountainous western united states. *Journal of Climate* **21** (23), 6404–6424.

Chai, T. & Draxler, R. R. 2014 Root mean square error (RMSE) or mean absolute error (MAE). *Geoscientific Model Development Discussions* **7** (1), 1525–1534.

Chang, S., Graham, W., Geurink, J., Wanakule, N. & Asefa, T. 2018 Evaluation of impacts of future climate change and water use scenarios on regional hydrology. *Hydrology and Earth System Sciences* **22** (9), 4793–4813. https://doi.org/10.1111/stan.12111.

Climate4impact 2023 https://climate4impact.eu/ (Accessed: 2 March 2023).

Climexp 2023 *Climate Explorer*. Available from: https://climexp.knmi.nl/start.cgi. (accessed 1 March 2023).

Doulabian, S., Golian, S., Toosi, A. S. & Murphy, C. 2021 Evaluating the effects of climate change on precipitation and temperature for Iran using RCP scenarios. *Journal of Water and Climate Change* **12** (1), 166–184. https://doi.org/10.5194/hess-22-4793-2018.

Easterling, D. R., Arnold, J. R., Knutson, T., Kunkel, K. E., LeGrande, A. N., Leung, L. R., Vose, R. S., Waliser, D. E. & Wehner, M. F. 2017 Precipitation change in the United States. https://doi.org/10.7930/J0H993CC.

Eden, J. M., Widmann, M., Maraun, D. & Vrac, M. 2014 Comparison of GCM-and RCM-simulated precipitation following stochastic postprocessing. *Journal of Geophysical Research: Atmospheres* **119** (19), 11–040. https://doi.org/10.1002/2014JD021732.

Gopal Shrestha, S. & Pradhanang, S. M. 2022 Optimal selection of representative climate models and statistical downscaling for climate change impact studies: a case study of Rhode Island, USA. *Theoretical and Applied Climatology*, 1–14. https://doi.org/10.1007/s00704-022-04073-w.

Gulizia, C. & Camilloni, I. 2015 Comparative analysis of the ability of a set of CMIP3 and CMIP5 global climate models to represent precipitation in South America. *International Journal of Climatology* **35** (4), 583–595. https://doi.org/10.1002/joc.4005.

Hersbach, H., Hirahara, S., Horányi, A., Muñoz-Sabater, J., Nicolas, J., Peubey, C., Radu, R., Schepers, D., Simmons, A., Soci, C., Abdalla, S., Abellan, X., Balsamo, G., Bechtold, P., Biavati, G., Bidlot, J., Bonavita, M., De Chiara, G., Dahlgren, P., Dee, D., Diamantakis, M., Dragani, R., Flemming, J., Forbes, R., Fuentes, M., Geer, A., Haimberger, L., Healy, S., Hogan, R. J., Hólm, E., Janisková, M., Keeley, S., Laloyaux, P., Lopez, P., Lupu, C., Radnoti, G., de Rosnay, P., Rozum, I., Vamborg, F., Villaume, S. & Thépaut, J.-N. 2020 The ERA5 global reanalysis. *Quarterly Journal of the Royal Meteorological Society* **146** (730), 1999–2049. https://doi.org/10.1002/qj.3803.

Hodson, T. O. 2022 Root-mean-square error (RMSE) or mean absolute error (MAE): When to use them or not. *Geoscientific Model Development* **15** (14), 5481–5487.

I CORE and CORE II 2023 Climate and ocean-variability, predictability, and change. *Atlantic* **10**, 41.

Immerzeel, W. W., Pellicciotti, F. & Bierkens, M. F. P. 2013 Rising river flows throughout the twenty-first century in two Himalayan glacierized watersheds. *Nature Geoscience* **6** (9), 742–745. https://doi.org/10.1038/ngeo1896.

Kaini, S., Nepal, S., Pradhananga, S., Gardner, T. & Sharma, A. K. 2020 Representative general circulation models selection and downscaling of climate data for the transboundary Koshi river basin in China and Nepal. *International Journal of Climatology* **40** (9), 4131–4149. https://doi.org/10.1002/joc.6447.

Kuttippurath, J., Murasingh, S., Stott, P. A., Balan Sarojini, B., Jha, M. K., Kumar, P., Nair, P. J., Varikoden, H., Raj, S., Francis, P. A. & Pandey, P. C. 2021 Observed rainfall changes in the past century (1901–2019) over the wettest place on Earth. *Environmental Research Letters* **16** (2), 024018.

Lutz, A., Biemans, H., ter Maat, H., Veldore, V. & Immerzeel, W. 2016a *Selection of Climate Models for Developing Representative Climate Projections for the Hindu Kush Himalayan Region*. Available from: http://hdl.handle.net/10625/57516.

Lutz, A. F., ter Maat, H. W., Biemans, H., Shrestha, A. B., Wester, P. & Immerzeel, W. W. 2016b Selecting representative climate models for climate change impact studies: An advanced envelope-based selection approach. *International Journal of Climatology* **36** (12), 3988–4005. https://doi.org/10.1002/joc.4608.

Ly, A., Marsman, M. & Wagenmakers, E.-J. 2018 Analytic posteriors for Pearson's correlation coefficient. *Statistica Neerlandica* **72** (1), 4–13. https://doi.org/10.1111/stan.12111.

Mahjour, S. K., Santos, A. A. S., Correia, M. G. & Schiozer, D. J. 2021a Scenario reduction methodologies under uncertainties for reservoir development purposes: distance-based clustering and metaheuristic algorithm. *Journal of Petroleum Exploration and Production Technology* **11** (7), 3079–3102. https://doi.org/10.1007/s13202-021-01210-5.

Mahjour, S. K., Santos, A. A. S., Santos, S. M. G. & Schiozer, D. J. 2021b Selection of representative scenarios using multiple simulation outputs for robust well placement optimization in greenfields. In *SPE Annual Technical Conference and Exhibition*? SPE, pp. D011S020R003. https://doi.org/10.2118/206300-MS.

Mendlik, T. & Gobiet, A. 2016 Selecting climate simulations for impact studies based on multivariate patterns of climate change. *Climatic Change* **135** (3), 381–393. https://doi.org/10.1007/s10584-015-1582-0.

Menebo, M. M. 2020 Temperature and precipitation associate with COVID-19 new daily cases: A correlation study between weather and COVID-19 pandemic in Oslo, Norway. *Science of the Total Environment* **737**, 139659. https://doi.org/10.1016/j.scitotenv.2020.139659.

Opała-Owczarek, M. & Niedźwiedź, T. 2019 Last 1100 yr of precipitation variability in western central Asia as revealed by tree-ring data from the Pamir-Alay. *Quaternary Research* **91** (1), 81–95. https://doi.org/10.1017/qua.2018.21.

Parding, K. M., Dobler, A., McSweeney, C. F., Landgren, O. A., Benestad, R., Erlandsen, H. B., Mezghani, A., Gregow, H., Räty, O., Viktor, E., El Zohbi, J., Christensen, O. B. & Loukos, H. 2020 GCMeval–An interactive tool for evaluation and selection of climate model ensembles. *Climate Services* **18**, 100167. https://doi.org/10.1016/j.cliser.2020.100167.

Paul, A. R. & Maity, R. 2023 Future projection of climate extremes across contiguous Northeast India and Bangladesh. *Scientific Reports* **13** (1), 15616. https://doi.org/10.1038/s41598-023-42360-2.

Peters, G. P., Andrew, R. M., Boden, T., Canadell, J. G., Ciais, P., Quéré, C. L., Marland, G., Raupach, M. R. & Wilson, C. 2013 The challenge to keep global warming below 2 C. *Nature Climate Change* **3** (1), 4–6. https://doi.org/10.1038/nclimate1783.

Pierce, D. W., Barnett, T. P., Santer, B. D. & Gleckler, P. J. 2009 Selecting global climate models for regional climate change studies. *Proceedings of the National Academy of Sciences* **106** (21), 8441–8446. https://doi.org/10.1073/pnas.0900094106.

Rosen, R. A. & Guenther, E. 2015 The economics of mitigating climate change: What can we know? *Technological Forecasting and Social Change* **91**, 93–106. https://doi.org/10.1016/j.techfore.2014.01.013.

Seager, R., Ting, M., Held, I., Kushnir, Y., Lu, J., Vecchi, G., Huang, H.-P., Harnik, N., Leetmaa, A., Lau, N.-C., Li, C., Velez, J. & Naik, N. 2007 Model projections of an imminent transition to a more arid climate in Southwestern North America. *Science* **316** (5828), 1181–1184. https://doi.org/10.1126/science.1139601.

Senatore, A., Fuoco, D., Maiolo, M., Mendicino, G., Smiatek, G. & Kunstmann, H. 2022 Evaluating the uncertainty of climate model structure and bias correction on the hydrological impact of projected climate change in a Mediterranean catchment. *Journal of Hydrology: Regional Studies* **42**, 101120. https://doi.org/10.1016/j.ejrh.2022.101120.

Seneviratne, S. I., Zhang, X., Adnan, M., Badi, W., Dereczynski, C., Di Luca, A., Vicente-Serrano, S. M., Wehner, M. & Zhou, B. 2021 11 Chapter 11: Weather and climate extreme events in a changing climate. *Bulletin of the American Meteorological Society* **104** (9), E1619–E1629.

Sillmann, J, Kharin, V. V., Zhang, X, Zwiers, F. W. & Bronaugh, D. 2013 Climate extremes indices in the CMIP5 multimodel ensemble: Part 1. Model evaluation in the present climate. *Journal of Geophysical Research: Atmospheres* **118** (4), 1716–1733. https://doi.org/10.1002/jgrd.50203.

Taylor, K. E., Stouffer, R. J. & Meehl, G. A. 2012 An overview of CMIP5 and the experiment design. *Bulletin of the American Meteorological Society* **93** (4), 485–498. https://doi.org/10.1175/BAMS-D-11-00094.1.

Thi Huong, N., Kim, Y.-T. & Kwon, H.-H. 2023 Evaluation and selection of CMIP6 GCMS for long-term hydrological projections based on spatial performance assessment metrics across South Korea. *Journal of Water and Climate Change* **14** (8), 2663–2679. https://doi.org/10.2166/wcc.2023.021.

Van Vuuren, D. P., Edmonds, J., Kainuma, M., Riahi, K., Thomson, A., Hibbard, K., Hurtt, G. C., Kram, T., Krey, V. J.-F., Masui, T., Meinshausen, M., Nakicenovic, N., Smith, S. J. & Rose, S. K. 2011 The representative concentration pathways: An overview. *Climatic Change* **109** (1), 5–31. https://doi.org/10.1007/s10584-011-0148-z.

Vincent, L. A. & Gullett, D. W. 1999 Canadian historical and homogeneous temperature datasets for climate change analyses. *International Journal of Climatology: A Journal of the Royal Meteorological Society* **19** (12), 1375–1388. https://doi.org/10.1002/(SICI)1097-0088(199910)19:12i1375::AID-JOC427¿3.0.CO;2-0.

Wang, T., Hamann, A., Spittlehouse, D. L. & Murdock, T. Q. 2012 Climatewna–High-resolution spatial climate data for Western North America. *Journal of Applied Meteorology and Climatology* **51** (1), 16–29. https://doi.org/10.1175/JAMC-D-11-043.1.

Wondmageghu Tenfie, H., Saathoff, F., Hailu, D. & Gebissa, A. 2022 Selection of representative general circulation models for climate change study using advanced envelope-based and past performance approach on transboundary river basin, a case of upper blue Nile Basin, Ethiopia. *Sustainability* **14** (4), 2140. https://doi.org/10.3390/su14042140.

You, L., Jiang, H., Hu, J., Chang, C. H., Chen, L., Cui, X. & Zhao, M. 2022 GPU-accelerated faster mean shift with Euclidean distance metrics. In: *2022 IEEE 46th Annual Computers, Software, and Applications Conference (COMPSAC)*. IEEE, pp. 211–216. https://doi.org/10.1109/COMPSAC54236.2022.00037.

Zwiers, F. W., Alexander, L. V., Hegerl, G. C., Knutson, T. R., Kossin, J. P., Naveau, P., Nicholls, N., Schär, C., Seneviratne, S. I. & Zhang, X. 2013 Climate extremes: Challenges in estimating and understanding recent changes in the frequency and intensity of extreme climate and weather events. *Climate Science for Serving Society: Research, Modeling and Prediction Priorities*, pp. 339–389. https://doi.org/10.1007/978-94-007-6692-1_13.

First received 20 September 2018; accepted in revised form 1 January 2018. Available online 30 January 2024